The effect of permafrost, vegetation, and lithology on Mg and Si isotope composition of the Yenisey River and its tributaries at the end of the spring flood

Vasileios Mavromatis[a,b*], Thomas Rinder[a], Anatoly S. Prokushkin[c], Oleg S. Pokrovsky[a,d,e], Mikhail A. Korets[c], Jérôme Chmeleff[a], Eric H. Oelkers[a.f]

[a] Géosciences Environnement Toulouse (GET), CNRS, UMR 5563, Observatoire Midi-Pyrénées, 14 Av. E. Belin, 31400 Toulouse, France

[b] Institute of Applied Geosciences, Graz University of Technology, Rechbauerstrasse 12, A-8010 Graz, Austria.

[c] V.N. Sukachev Institute of Forest, SB RAS, Akademgorodok 50/28, Krasnoyarsk 660036, Russia

[d] BIO-GEO-CLIM Laboratory, Tomsk State University, Tomsk, Russia

[e] Institute of Ecological Problems of the North, RAS, 23 Naber. Sev. Dviny, Arkhangelsk

[f] Earth Sciences, University College London, WC1E 6BT, United Kingdom

*Corresponding author: E-mail address: mavromatis@tugraz.at

Abstract

This work focuses on the behavior of the stable Mg and Si isotope compositions of the largest Arctic river, the Yenisey River and 28 of its major and minor tributaries during the spring flood period. Samples were collected along a 1500 km latitudinal profile covering a wide range of permafrost, lithology, and vegetation. Despite significant contrasts in the main physico-geographical, climate, and lithological parameters of the watersheds, the isotope composition of both dissolved Mg and Si was found to be only weakly influenced by the degree of the permafrost coverage, type of vegetation (forest vs. tundra), and lithology (granites, basalts, carbonates or terrigenous rocks). This observation is generally consistent with the lack of chemical uptake of Mg and Si by soil mineral formation and vegetation during the early spring. The radiogenic Sr isotope composition of the Yenisey and its tributaries varied within a narrow range ($0.708 \leq {}^{87}Sr/{}^{86}Sr \leq 0.711$) reflecting the dominance of Phanerozoic rock weathering and/or atmospheric deposition on these compositions. The Mg and Si isotopic compositions of riverine samples reflect two main processes with distinct isotopic signatures. First, isotopically heavier Mg ($\delta^{26}Mg$ = -1.0 ± 0.2 ‰) and isotopically lighter Si ($\delta^{30}Si$ = 1.0 ± 0.25 ‰) are added to the waters by river suspended matter dissolution and leaching from vegetation biomass/topsoil litter. Second, isotopically lighter Mg ($\delta^{26}Mg$ = -1.5 to -1.75 ‰) and isotopically heavier Si ($\delta^{30}Si$ = 1.75 to 2.0 ‰) are delivered to the Yenisey's tributaries from deep underground water feeding the rivers via taliks. This lighter Mg and heavier Si isotopic composition is interpreted to originate from Precambrian dolomite dissolution and aluminosilicate dissolution coupled with authigenic mineral precipitation, respectively, in deep underground water reservoirs. Taking account of the isotopic composition evolution over the course of the year established earlier on mono-lithological watersheds of the Yenisey basin, the average annual isotopic signatures of the Yenisey river arriving to the Arctic Ocean are estimated to be $\delta^{26}Mg$ = -1.58±0.30 ‰ and $\delta^{30}Si$ =+1.60±0.25 ‰. As the Yenisey is the largest river feeding the Arctic Ocean and as it

samples a large variety of environments and lithologies, these values may be reasonable

estimates for the average Mg and Si isotopic composition of the dissolved riverine flux to the

Arctic Ocean.

1. Introduction

Fresh water input to the Arctic Ocean is mainly provided by the riverine systems draining Siberia; discharge from the Canadian Arctic shelf contributes less than 15% of the total water volume arriving to the Arctic Ocean (Holmes et al., 2012, 2013). Over the past two decades, numerous studies of large river systems flowing into the Arctic have examined the chemical composition of water samples collected during the summer (July-August) (Huh et al., 1998a,b; Huh and Edmond, 1999; Vigier et al., 2001; Pokrovsky and Schott, 2002; Gordeev et al., 2004; Millot et al., 2003; Pokrovsky et al., 2005a; Lemarchand and Gaillardet, 2006; Andersen et al., 2007). These studies provide significant information about the processes controlling element transfer to the ocean and have allowed the characterization of the major element biogeochemical cycles in boreal regions. Nevertheless, the fresh water discharge in Arctic Ocean exhibits strong seasonal variability. Approximately 45 % of the annual water discharging into the Arctic occurs during the spring snowmelt (Holmes et al., 2013). This observation has a major impact on both the quantity of dissolved elements transferred to the Arctic Ocean and their isotopic composition. The present study was designed to assess the contribution of the spring flood to the chemical and isotope input to the Arctic Ocean from the Yenisey river and its main tributaries.

Studies on small boreal rivers in Sweden and in Alaska (Guo et al., 2004; 2012) demonstrated that elemental fluxes in the Arctic region vary seasonally as does water discharge. As the Yenisey River is the largest contributor of freshwater to the Arctic Ocean, providing 18% of the total annual river discharge (Holmes et al., 2013), evaluation of its elemental fluxes, isotopic signatures, and their possible origin is especially significant for characterizing weathering processes and the Arctic Ocean chemistry. Moreover, the Yenisey is the most important river feeding the Arctic Ocean in terms of silicate weathering and carbon drawdown; from 39 to 55% of the silicate weathering and from 45 to 61% of the

carbonate weathering of the rivers draining into the Arctic Ocean occurs in the Yenisey catchment (Tank et al., 2012).

Owing to its unique geographic position, sampling a latitudinal transect of the Yenisey River allows the detailed study of the influence of numerous factors on river water dissolved load as well as its isotopic composition. Roughly 88 percent of the Yenisey river watershed is covered with permafrost. Its tributaries drain highly contrasting basins: its left tributaries drain western Siberian bogs and peat soils and its right tributaries drain regions of variable lithology, from granites/gneisses in the south to carbonate and terrigenous rocks in the middle, and basalts and tuffs in the north. The tributaries also have contrasting land cover, both in terms of vegetation (evergreen needle-leaf, deciduous broadleaf, and deciduous needle-leaf forests) and the relative contribution of wetlands (0-20%), tundra (0-100%), and forest (0-100%) (see Tables S1 and S2 of the Electronic Supplementary Material, ESM).

The major element concentrations and discharge of large Arctic Rivers can be constrained using the data summarized by Gordeev et al. (1996) and Holmes et al. (2012, 2013). For the case of the Yenisey River, the spring flood (May-June) contributes 29.0 ± 1.4 % and $38.6 \pm 2.3\%$ of the annual flux of Mg and Si, respectively. These values are calculated based on mean multi-annual fluxes and concentrations provided in ESM Table S3 and S4. This study was designed to quantify the Si and Mg isotopic composition and to constrain the processes influencing these compositions during the critical spring flood period.

Previous studies of small and medium permafrost-affected monolithological watersheds covered by monospecific (larch-free) forests developed on Central Siberian basalts help to illuminate processes affecting major element dissolved riverine fluxes during the spring floods. During the ice break and following massive freshet, radiogenic Sr signatures evolve towards the atmospheric value, suggesting a major influence of dust dissolution on water chemistry (Bagard et al., 2011, 2013). Stable Si isotope ratios decrease at the beginning of the spring flood, suggesting the dissolution of Si-bearing clays present in the

river suspended matter (RSM) (Pokrovsky et al., 2013). Another factor influencing the Si isotopic composition of Siberian rivers is plant litter leaching, which tends to make the river water $\delta^{30}Si$ more positive, as plant litter is 1 to 2 ‰ more positive than the clay minerals (Opfergelt et al., 2008).

Numerous earlier studies have used Mg isotope signatures in riverine waters to track weathering processes as Mg isotopes exhibit distinct fractionation during weathering (Tipper et al., 2008; 2012; Wimpenny et al., 2010; 2014; Pogge von Strandmann et al., 2008; Brenot et al., 2008; Oelkers et al., 2015). In particularly, in silicate catchments the Mg isotope compositions of riverine waters generally exhibit lighter compositions compared to their host rock; this behavior has been attributed to the preferential uptake of heavy Mg during secondary silicate mineral formation (Teng et al., 2010; Opfergelt et al., 2012, 2014; Beinlich et al., 2014; Pogge von Strandmann et al., 2008).

The Mg isotope signatures of Siberian rivers have the potential to trace both secondary mineral formation in soil and underground horizons, and the contribution of bedrock dissolution. As a working hypothesis, we might expect that the effect of rock lithology and plant litter leaching / uptake on Yenisey river chemistry will progressively decrease northward, given that the mineral soil column and the rooting zones are frozen in continuous permafrost. In contrast, silicate RSM dissolution in the river water will be controlled by the RSM concentration; as most of the RSM originates from river bank abrasion and its contribution to river chemistry will be less sensitive to the degree of permafrost coverage and basement lithology. Moreover the composition of the RSM is likely variable throughout the year; during the spring flood period, only the upper organic-rich soil layers are unfrozen and can deliver particulate material to the river (Pokrovsky et al., 2013, 2015a; Viers et al., 2015). The role of these processes will be tested in this study. It is anticipated that by providing quantitative constraints on the major element sources it may be possible to better predict the effect of future global change on the chemical and isotopic fluxes to the Arctic Ocean.

2. Water Sampling and Analytical Procedures

2.1 Sampling Area

The river water samples examined in this study were collected during a Yenisey River cruise on the river-sea class ship "Sovetskaya Arktika" between the 12th and the 28th of June, 2012. The cumulative distance covered by the ship was more than 3,000 km. During the expedition, samples were collected from the main Yenisey River channel and all of its significant tributaries, including 9 draining the western and 16 draining the eastern parts of the basin (see Fig. 1 and Table 1). Among these were three major tributaries: the Angara, the Podkamennaya Tunguska, and the Nizhnyaya Tunguska, representing 25, 10, and 19%, respectively, of the annual Yenisey river discharge to the Kara Sea. Based on the Roshydromet network of 15 gauging stations, it is estimated that the sampled tributaries contribute ~79% of the annual discharge of Yenisey River to Kara Sea. In addition, 3 sampling stations were established within the Nizhnyaya Tunguska River basin; these tributaries drain both the northern (i.e. the Putorana Plateau) and southern parts of the Central Siberian Platform (i.e. the Yerachimo, Severnaya, and Letnyaya Rivers). Note that Yerachimo is a tributary of Nizhnyaya Tunguska River and is not directly connected to Yenisey River.

The sampled tributaries are located along a 1500 km latitudinal transect from S to N and sample watersheds of distinct sizes, geomorphology, permafrost extent, lithology, climate and vegetation (see Table 1 and ESM Tables S1 and S2). The total watershed area of the rivers sampled in this work is about 1.75 million km^2, representing 68% of entire Yenisey River basin. Permafrost ranges from non-permafrost in south to continuous permafrost in the north (Brown et al., 1998). The mean annual air temperatures (MAAT) along the transect range from - 0.01 to - 11.30°C (0.5º×0.5º grid data, CRU TS3.2 available at Mitchell and Jones, 2005).

2.2 Sample collection

Tributary river waters were sampled from motorboats a few kilometers above their confluences with the main Yenisey River channel. Water samples were collected in the middle stream of the tributaries just beneath the water surface for the smaller rivers or at several depths using hand-made pump to obtain depth integrated samples for the larger rivers. Yenisey river water was sampled at 8 stations: Maliy Yenisey River headwater samples were collected at 2 stations in the middle of the river just beneath the water surface, and the main channel of the Yenisey River was collected at 6 stations (from 58° to $\sim 70^{o}$N) using a D-96 sampler equipped with Teflon nozzles and Teflon sample collection bags to obtain depth-integrated and flow-weighted samples. A shipboard laboratory allowed sample filtration (pre-combusted Whatman glass fiber filters (GFF), 0.7 µm nominal pore size) and sample preservation to be performed promptly under clean conditions. Water temperature, pH, SpCond, turbidity, and dissolved O_2 were measured directly in the rivers using a multiparameter sonde YSI-6 (YSI, USA). From 5 to 10 L of river water was collected; these samples were immediately filtered, collected in Nalgene high-density polyethylene bottles, acidified with ultrapure nitric acid, and stored in a refrigerator prior to analyses. River suspended matter (RSM) concentration was measured by filtering 0.5-1.0 L of river water on pre-weighted GFF or acetate cellulose filters (< 0.22 µm) with an uncertainty of 10%. A large quantity of RSM was collected from the main river and its tributaries by sedimentation in 50-L PVC barrels, decanted for 1 week, centrifuged, and freeze-dried.

3. Chemical and Isotopic Analyses

The concentrations of major cations, including Mg, in acidified water samples were measured by ICP-MS (Agilent 7500ce) at the GET laboratory (Toulouse, France). Indium and rhenium were used as internal standards to correct for instrument drift and potential matrix effects. In addition, Mg was analyzed by atomic absorption spectroscopy with an uncertainty

of 1% and a detection limit of 10 µg kg^{-1}. A non-acidified water sample was used for: 1) Si determination via the ammonium molybdate method using a Bran+Luebbe AutoAnalyser 3 with a ±2 % uncertainty and a 10 µg kg^{-1} detection limit, 2) dissolved organic (DOC) and inorganic (DIC) carbon analyses by total combustion at 800°C using a SHIMADZU Pt catalyser (TOC-V$_{CSN}$) with a 5 % uncertainty and a detection limit of 0.1 mg kg^{-1} (see Prokushkin et al., 2011); and 3) chloride and sulfate determination via liquid chromatography using a DIONEX ICS-2000 with an uncertainty of 2 % and a detection limit of 0.02 mg kg^{-1}. The SLRS-5 international river water standard was used to check the accuracy of the Si, Mg, Ca, and Sr analyses. The differences between the certified or recommended values and our measurements were lower than 10%. The concentration of colloidal (1 kDa – 0.45 µm) and dissolved or low molecular weight (LMW, < 1 kDa) forms of Si and Mg were measured by on-site dialysis as described by Bagard et al. (2011) and Pokrovsky et al. (2013).

Water samples were chemically purified prior to Mg isotopic analysis by cation exchange chromatography. Separation of the Mg from the matrix elements followed the protocol described by Mavromatis et al. (2013) using AG50W-X12 resin eluted with 1.0 M HNO$_3$. The yields after chromatographic separation were better than 99 % of the total Mg loaded in the columns with the cation/Mg ratio in the sample <0.05 and thereby avoiding potential interference and matrix effects in the mass spectrometry analyses. Magnesium isotopic ratios were measured using a Thermo-Finnigan 'Neptune' Multi Collector Inductively Coupled Plasma Mass Spectrometer (MC-ICP-MS) at the GET laboratory (Toulouse, France) in low-resolution mode. All analyzed fluids were prepared in 0.3 M aqueous HNO$_3$ and introduced into the Ar plasma with a standard spray chamber. Instrumental mass fractionation effects were corrected by sample-standard bracketing, and all results are presented in delta notation relative to the DSM3 reference material as: [δ^{x}Mg= ((^{x}Mg/^{24}Mg)$_{sample}$ / (^{x}Mg/^{24}Mg)$_{DSM3}$ -1)×1000)] where x is the Mg mass of interest. All results are consistent with mass-dependent fractionation (see Table 2). The reproducibility of the

δ^{26}Mg analyses, assessed by replicate analyses of the DSM-3, CAM-1 and OUMg Mg reference standards, and the dolomite carbonate standard JDo-1 was better than 0.02‰, 0.07‰, 0.06‰ and 0.09‰, respectively. This precision is similar to that reported earlier from our laboratory (Pearce et al., 2012; Beinlich et al., 2014; Mavromatis et al., 2012; 2013; 2014a; 2014b; Shirokova et al., 2013; Schott et al., 2016), and fall within the range of values reported earlier for these standards by other groups (Li et al., 2012; 2014; Tipper et al., 2006; Bolou-Bi et al., 2009; Geske et al., 2015; Immenhauser et al., 2010; Pogge von Strandmann, 2008; Wombacher et al., 2009, 2011). In addition the column chemistry of the IAPSO seawater sample provided results similar to those reported by Wombacher et al., (2011) (see Table 2).

Si was purified from the river water matrix following the protocol described by Pokrovsky et al. (2013). Briefly, river water samples were reacted with 2% HNO_3 and 1% H_2O_2 to remove as much dissolved organic matter as possible. If necessary the resulting solution was concentrated via evaporation to obtain a Si concentration of 3 ppm. The final sample was acidified with bidistilled HCl to achieve a 0.05M matrix prior to its loading onto a 1.6 mL cation exchange resin BioRad 50W-X12, 200 to 400 mesh in H^+ form. The isotope analyses were carried out using a 'Neptune' MC-ICP-MS at the GET laboratory (Toulouse, France) in medium resolution mode. At least three replicate samples were measured against the NBS-28 standard. The basalt standard BHVO-2 was treated similar to the water samples described above and it was measured 18 times during the analyses, resulting in a δ^{29}Si of -0.16 ±0.02‰ and a δ^{30}Si of -0.29 ±0.04 ‰.

The ^{87}Sr/^{86}Sr ratios of the water samples were measured using a VG Sector 54 thermal ionization mass spectrometer (TIMS). Liquid samples were evaporated, taken up in 3M aqueous HNO_3 and run through Sr-spec columns. The purified Sr was then loaded onto outgassed Ta filaments. The samples were run at ^{88}Sr beam potentials of 2V and 100 ratios were collected using a multi-dynamic peak jumping routine. Resulting ^{87}Sr/^{86}Sr ratios were

normalized to an $^{86}Sr/^{88}Sr$ ratio of 0.1194. Six analyses of the NBS987 standard yielded an average $^{87}Sr/^{86}Sr$ of 0.710220±0.000011 (2SD). Individual errors did not exceed ±0.000011 $^{87}Sr/^{86}Sr$. Total blanks for Sr were found to be negligible compared to the Sr masses of the samples.

Speciation calculations were conducted using Visual Minteq 3.1 software (Gustafsson, 1999), version 3.1 (October 2014) for Windows, (see Unsworth et al. (2006) for a vMINTEQ application example) in conjunction with the Stockholm Humic Model (SHM), which accounts for aqueous Fe and Al complexation with dissolved organic matter. In addition, the PHREEQC code, together with its lnll database (Parkhurst and Appelo, 1999), was used for calculating the fluid sample saturation states with respect to various clay minerals. Regression and power functions were used to examine the relationships between element concentrations, isotope ratios, and the main physico-geographical parameters such as MAAT, permafrost coverage, watershed size, watershed average latitude, % of wetland versus tundra and forest coverage, RSM concentration and proportion of various rock type on the watershed. These regressions were performed using the least squares method, Pearson correlation, and a one-way ANOVA with STATISTICA version 8 software (StatSoft Inc., Tulsa, OK). Correlation coefficients were calculated to elucidate the relationships between the dissolved element concentrations and ratios (DOC, DIC, Mg, Ca, Si, Al) with the isotopic signatures of the Yenisey tributaries.

4. Results

4.1. The major chemistry and Sr isotope ratio of the Yenisey River and its tributaries during the spring flood

The chemical composition of major elements in all river water samples can be found in Table S5. A plot of Mg/(Na+K) vs. Ca/(Na+K) concentrations of the sampled river waters

is shown in Fig. 2. The linear trend of the data on this plot suggests that they are consistent with the mixing of two or more end members such as Precambrian dolomite, basalts, granites and larch litter. Similar observations of the chemistry of Siberian rivers were attributed by Bochkarev (1959), Alekin (1970), and Pokrovsky et al. (2006) to the mixing of chemical inputs from two major sources. The first is the surface organic-rich soil layer together, including plant litter, and the second is the dissolution of deep mineral soil horizons and base rock occurring in underground water reservoirs that feed the river via taliks (Anisimova, 1981; Bagard et al., 2011, 2013). The relative contribution from these two pools varies over the year, owing to the presence of permafrost. In particular, top soil and plant litter leaching dominates during the early spring, whereas the mineral soil horizons are more reactive at the end of the summer when the thickness of the thaw layer is at its maximum; the weathering of the rock basement is most pronounced during winter baseflow. Finally the annual atmospheric input contribution to the Yenisey and its tributaries is below 10% (Pokrovsky et al., 2005), which is significantly different from the conditions occurring to the West as the Karelia and the Kola regions are located closer to the sea coast.

The $^{87}Sr/^{86}Sr$ ratio is an efficient tracer of bedrock weathering especially in permafrost-affected zones (Keller et al., 2010; Bagard et al., 2011; 2013). Despite a significant variation of Sr concentration in sampled rivers, ranging from 13 to 350 µg kg^{-1}, the majority of sampled tributaries (excluding M5 Garevka, see below) exhibit $^{87}Sr/^{86}Sr$ ratios (Fig. ESM-1), ranging from 0.708 to 0.711, with an average value of 0.7087±0.0004. This value also coincides with this ratio at the mouth of the Yenisey (0.7088) as well as along the main course of the river.

Plots of Sr isotope ratio as a function of all available physico-geographic parameters including watershed size, latitude, MAAT, permafrost coverage, forest, bog, and tundra proportion of the watershed, and rock lithology (i.e. carbonates, granites, basalts and terrigenous rocks) did not reveal any statistically significant (at $p < 0.05$) relationship (see

ESM Figs. S1-S6). Only a small tributary, the Garevka, exhibited a highly radiogenic $^{87}Sr/^{86}Sr$ value, equal to 0.728. This elevated number may stem from a dominance of late Archean - early Proterozoic granites in this watershed. Likewise, the plot of the $^{87}Sr/^{86}Sr$ ratio versus the percent of basalt in the watershed, shown in Fig. 3, suggests a mixture of a "young" Permo-Triassian basaltic endmember and an "old" basalt-free endmember corresponding to late Proterozoic – Cambrian carbonates, granites, and terrigenous rocks.

The $^{87}Sr/^{86}Sr$ ratios of the Yenisey River and its tributaries are within the range reported for Eastern Siberian rivers (Huh et al., 1998a, b; Huh and Edmond, 1999) and slightly lower those of the Yenisey coastal sediments (0.712; Guo et al., 2004), the average value of Canadian rivers (0.7111; Wadleigh et al., 1985), and the global river average which range from 0.7116 (Pearce et al., 2015) to 0.7119 (Palmer and Edmond, 1989).

4.2 The Mg isotope composition of Yenisey River water

The Yenisey River tributary water samples exhibit variations of up to 1‰ in $\delta^{26}Mg$ (see Table 2). The main channel of the Yenisey River water is enriched in heavier Mg by about 0.3‰ moving northwards from ~51-52°N to 60°N but remains constant north of 60°N (ESM Fig. S7), with a $\delta^{26}Mg$ composition of -1.3‰ close its delta. The most ^{26}Mg enriched samples were collected from the Yerachimo and the Nizhnyaya Tunguska, both of which drain the Central Siberian basalt province, and most northern, tundra-dominated M Kheta tributary. Note that the $\delta^{26}Mg$ composition of the Nizhnyaya Tunguska mouth water sample is identical to that reported by Mavromatis et al. (2014a) for the late spring, high flow waters collected during the years 2008 and 2009. The samples most enriched in ^{24}Mg were from the Vorogovka, the Miroedikha, and the Letnyaya.

The Mg isotope signatures were found to be independent of most watershed physico-geographic parameters including the basin area, MAAT, % of forest, wetland and tundra on the watershed, and the lithological composition of the watersheds such as the proportion of

granites, basalts, terrigenous, and carbonate rocks as illustrated in ESM Figs. S8-S12 and summarized in ESM Table S6; this table also lists of all correlation coefficients. Note that no statistically significant variation of Mg isotope composition with DOC concentration was observed ($p < 0.05$). The lack of Mg transport via organic colloids is confirmed by dialysis results suggesting that less than 10% of the Mg was present in colloidal (1 kDa − 0.45 µm) form. Note also that it was previously shown that no fractionation occurs between Mg complexed in DOC and free Mg (Illina et al., 2013). In contrast, the dissolved inorganic carbon (DIC) concentration exhibited a clear negative correlation with $\delta^{26}Mg$ ($p = 0.03$, $R^2 = 0.8$) as shown in Fig. 4A. A similar correlation between $\delta^{26}Mg$ and total dissolved solids was observed previously for the Mackenzie River basin that also drains permafrost regions (Tipper et al., 2012). The increase of river suspended matter concentration also exhibits a weak relation with the Mg isotopic ratio in the river water ($R^2 = 0.18$, $p = 0.03$). Moreover as illustrated in Fig. 4B, $\delta^{26}Mg$ exhibits a positive correlation with 1/Mg ($R^2 = 0.7$, $p > 0.05$), excluding samples collected from the Garevka and Yerachimo tributaries. It should be emphasized that Garevka is strongly influenced by granites and Yerachimo is not a direct tributary of Yenisey River. Note that due to the large spatial scale of this study, the observed chemical trends may be affected by some dilution and/or concentration effects.

4.3 Si isotope variations of water samples

The measured water samples exhibit variations of up to 1.5‰ in $\delta^{30}Si$ (see Table 2). Similar to the behavior of Mg isotopes, a slight progressive enrichment in ^{30}Si is observed northwards along the Yenisey River (ESM Fig. S13), with the $\delta^{30}Si$ composition of the most northern sampling point equal to 1.3 ‰, which is 0.2‰ heavier than that collected from the southernmost station. The water samples collected from the Yenisey River tributaries exhibited $\delta^{30}Si$ variations, up to 1.4 ‰. The water samples collected from the Komsa, the Miroedikha, and the Sukhaya Tunguska tributaries exhibited the largest depletion in ^{28}Si, with

δ^{30}Si values of 2.11‰, 2.01‰ and 1.97‰, respectively. The samples most enriched in ^{28}Si were collected from the tributaries draining the western Siberia lowland specifically from the Sym, the Kas, and the Turukhan with δ^{30}Si values of 0.75 ‰, 0.93 ‰ and 0.92 ‰, respectively.

Similar to Mg, the Si isotope signatures were found to be statistically independent of most watershed physico-geographic parameters including the basin area, MAAT, % of forest, and tundra, and the watershed lithological composition including the proportion of granites, basalts, terrigenous, and carbonate rocks as illustrated in ESM Figs. S14-S18 – see Table S6 for a list of correlation coefficients. Note however, that a weak correlation (R=0.23, p=0.01) can be seen between δ^{30}Si and wetland coverage. The Si isotopic composition, became significantly lighter with increasing RSM concentration. According to SEM observations and EDX analyses, the mineralogical composition of the RSM in the sampled rivers consists of amorphous Al-Si-allophanes rich in organic carbon, illite, chlorite, montmorillonite, quartz, feldspars, amphibole, and mica. A significant diatom concentration was observed by SEM in the Vorogovka and Bakhta tributaries. Diatoms are known to preferentially uptake light Si (De La Rocha et al., 1997). The presence of diatoms, however, was not correlated with any measured isotopic signature.

5. Discussion

5.1. Mg isotopic signals in riverine waters: effect of silicate RSM leaching and deep carbonate rock dissolution

Permafrost extends throughout the Yenisey drainage basin, but ranges from continuous in the north to isolated and sporadic in the south (Fig. 1; ESM Table S1). Note that only the Kem and Kas river basins, located in the southwestern part of the Yenisey catchment, are not affected by permafrost. Despite the contrasting permafrost distribution, no significant correlation was observed between the isotopic compositions and permafrost extent, as well as

the MAAT (see ESM Figs. S3, S4, S9, S10, S15, S16). As mentioned above, previous studies argued that the major chemistry of Siberian Rivers originates from the combination of two sources (Bochkarev, 1959; Alekin, 1970; Pokrovsky et al., 2006). The first is the surface organic-rich soil layer including plant litter. The second is the dissolution of minerals deep within soils and in the base rock fed to the river via taliks (Anisimova, 1981; Bagard et al., 2011, 2013). The relative contribution from these two pools is variable over the year, owing to the presence of permafrost. In particular, top-soil and plant litter leaching occurs mainly during the early spring, whereas mineral dissolution is particularly active at the end of the summer, when the thickness of the thaw layer maximizes, and rock basement weathering is most pronounced during winter baseflow.

The Mg isotopic composition of two large Central Siberian rivers (the Kochechum and the Nizhnyaya Tunguska) was recently measured to illuminate the Mg sources generated by basalt weathering under permafrost conditions in a larch deciduous forest (Mavromatis et al., 2014a). During the winter, the dissolved Mg isotope composition of these rivers was significantly lighter than the surface basaltic rocks and the atmospheric deposition, suggesting either a deep underground source such as sedimentary carbonate rocks or the non-conservative transfer of basaltic Mg to the fluid phase. Overall the riverine waters were 0.6-1.0 ‰ lighter than the unaltered bedrock and deep minerals in the soil horizons. During the spring flood and in the summer-fall season, δ^{26}Mg increases by 0.2-0.3 ‰ and approaches the Mg isotope composition of the ground vegetation (dwarf shrubs, mosses) and the soil organic horizon. It seems likely that during the spring high flow sampling period, the dissolved load mainly originated from the soil surface, RSM, and plant litter, as the mineral soil layer is entirely frozen. Indeed as it can be seen in Fig. 5A, a correlation (R^2=0.5, p<0.05) exists between the increasing RSM load between 0 and 15 mg/L and ^{24}Mg depletion in the fluid samples. Another correlation, however, is seen between δ^{26}Mg and the dissolved inorganic carbon concentration of riverine water samples (Fig. 4A). This trend allows the distinction

between Mg originating from silicate and carbonate sources. Specifically, silicate rocks and plant litter will tend to liberate Mg but add little DIC (Mavromatis et al., 2014a),whereas Precambrian carbonate rock dissolution will add significant DIC; waters originating from the latter source hve been observed to exhibit δ^{26}Mg ranging from -1.5 to -2.2 ‰ (Pokrovsky et al., 2011). The linear correlation of δ^{26}Mg and DIC apparent in Fig. 4A suggests a binary mixing of two end-members, that can be described by:

$$\delta^{26}\text{Mg} = A \times \text{DIC} - B, \text{R}^2=0.78; p=0.03 \tag{1}$$

where $A = -0.0345$, $B = 0.9206$ and δ^{26}Mg is given in per mil and DIC in ppm.. Solving this equation for a DIC concentration of 35 ppm as is reported by Bagard et al. (2011) which corresponds to the highest contribution of dolomite rocks to the river water assessed during winter baseflow for the Nizhnyaya Tunguska yields a δ^{26}Mg of -2.1‰. This value is consistent with the δ^{26}Mg composition of dolomite rocks present in the upper reaches of the Nizhnyaya Tunguska river basin (Pokrovsky et al., 2011). During the spring flood, river waters are undersaturated with respect to Mg-bearing carbonates (S.I. < -1, ESM Table S6), thus the dissolution of the isotopically heavy Mg sources (e.g. surface silicate rocks, soil plant litter) may occur without significant isotope fractionation caused by secondary carbonate mineral precipitation (Pearce et al., 2012; Mavromatis et al., 2015). This process would provide heavy Mg at relatively low DIC, which is typical for spring waters. An acid spring pulse, fairly well known in Scandinavian rivers (Buffam et al., 2008) and linked to fast leaching of organics from the vegetation, is also responsible for the low DIC in the river water during this period. This is most evident for the Yenisey tributaries draining the western Siberian bogs and wetlands including the Kas, the Elogyi, the Turukhan, the Sym, and most northern Bolshaya Kheta basin areas. These rivers drain primarily peat deposits, where surface waters have little contact with soil mineral horizons (Pokrovsky et al., 2015b). This binary mixing model is further supported by the correlation of δ^{26}Mg with 1/Mg concentration

plots as can be seen in Fig. 4B. Note that the observed binary mixing does not necessarily exclude the mixing of several endmembers as previously suggested for the Mackenzie Basin (Tipper et al., 2012). As shown by Zakharova et al. (2007) in boreal rivers, the Ca+Mg flux increases in the order carbonates > basalts > litter > granites > aerosols, but their compositions fall on the same linear trend on δ^{26}Mg versus 1/Mg concentration plots. Moreover, the δ^{26}Mg composition of basalts, granites and plant litter is very similar (see Mavromatis et al., 2014a). Indeed, it can be seen from the Ca/(Na+K) vs Mg/(Na+K) plot of the studied rivers (Fig. 2) that several possible sources of the major cations are aliened along the same trend. Therefore, the compositional trends observed during the spring flood do not allow discrimination between the organic and mineral pools of Mg feeding the river, and measurements during the winter season are necessary to constrain the underground (carbonate, silicate) source of riverine Mg.

Basaltic rocks are generally depleted in ^{24}Mg with an average δ^{26}Mg = - 0.23 ± 0.11‰ (Teng et al., 2007; Handler et al., 2009; Bourdon et al., 2010) compared to carbonates that are generally enriched in ^{24}Mg. The dolomites from the Patom Paleobasin, drained by the eastern Yenisey tributaries (the Nizhnyaya Tunguska and Podkamennaya Tunguska rivers) are as light as -2.5‰ (Pokrovsky et al., 2011). This observation shows that the host rock can exert a significant effect on the isotopic composition of the dissolved Mg; a strong influence of carbonate dissolution has been observed in the Central Siberian river basins at the end of the winter season (Mavromatis et al., 2014a). Indeed, the Precambrian dolomites present in the southern part of the Siberian platform, provide 30 to 40 ppm of DIC at the end of the winter to the Nizhnaya Tunguska River (Bagard et al., 2011; Prokushkin et al., 2011). This feeding of the main river occurs via deep taliks, where the interaction of dolomite with basement fluids could occur.

5.2. The effect of RSM and alumino-silicate mineral precipitation in deep reservoirs on Si isotope signatures:

Heavy Si isotopic compositions are typical for Central Siberian rivers during the winter; Si is typically 1 to 1.5‰ lighter during the spring floods. At the discharge maximum, which occurs during the spring flood, typically at the beginning of June, the δ^{30}Si of the Nizhnaya Tunguska and the Kochechum river water approaches that of the particulate suspended matter and weathered basalt (i.e. 0.25±0.16 and 0.32±0.13 ‰, respectively, see Pokrovsky et al., 2013). The concentrations of dissolved Si in Central Siberian riverine waters decrease by a factor of 2.5 to 3 at the beginning of June compared to the winter baseflow, whereas the river discharge increases by 2 to 3 orders of magnitude (Pokrovsky et al., 2013). Owing to extensive permafrost, most of the soil is still frozen and so little to no subsoil fluid contribution to the rivers is expected to occur during the spring flood period. Hence the overall Si concentration in riverine waters is dominated by Si-bearing solids present at the soil surface, on the river banks, or within the melting snow. Such solids likely include Al-allophane, smectite, plant debris, and plant litter present in the topsoil horizons. The riverine δ^{30}Si values of the Kochechum and Nizhnyaya Tunguska rivers are their lightest at the beginning of June, during the late spring flood, when the soil horizons in the watershed remain frozen.

The impact of silicate mineral dissolution and precipitation on the Si isotope ratio in sampled river water can be assessed with the aid of Fig. 6. The correlation of low Ca/Al ratios with high δ^{30}Si shown in Fig. 6A, suggests clay mineral formation in the deep groundwaters of the watersheds. Indeed, secondary clay mineral formation is considered to be a key fractionation process controlling the δ^{30}Si composition in natural waters (Georg et al., 2006). Clay mineral formation leads to high δ^{30}Si due to the preferential uptake of ^{28}Si by secondary Si-bearing phases (Georg et al., 2006). This is reflected in the δ^{30}Si composition of soil solution samples from the Nizhnyaya Tunguska basin, which exhibit values of 2.0±0.1‰

(n=3) (Pokrovsky et al., 2013). Moreover, clay precipitation would remove Al relative to Ca from aqueous fluids (De la Rocha et al., 2000). We thus hypothesize that the Yenisey tributaries exhibiting high Ca/Al and heavier Si (e.g. Miroedikha, Letnyaya, Sukhaya Tunguska, Yerachimo) are strongly affected by winter groundwaters that were influenced by secondary silicate clay formation. This observed [30]Si enrichment is typical for permafrost dominated rivers such as the Nizhnyaya Tunguska and the Kochechum during winter baseflow, as during this time the deep groundwaters feeding the rivers have longer residence times, allowing for a longer interaction with their surrounding rocks leading to clay precipitation (Pokrovsky et al., 2013).

The maximum concentration of Al in the rivers of the Yenisey basin is achieved during the spring flood, when it is present in organic colloids (Bagard et al., 2011). Note that Al is fully complexed with Dissolved Organic Matter (DOM; Pokrovsky et al., 2015b) in the left tributaries of the Yenisey River. Our calculations also demonstrate the dominance (>95%) of Al-DOC complexes in surface waters. Aluminium therefore becomes mobile in the surface environments due to the presence of DOM. This is not the case for DOM-poor underground waters where Al precipitates as secondary clays thus increasing the Ca/Al ratio in the remaining fluids.

The waters of some of the Yenisey tributaries exhibit depleted [30]Si isotopic signatures, low Ca/Al, Ca/Si and Mg/Si concentration ratios, and high RSM (see Fig 6). Such observations can be attributed to the dissolution of RSM components such as allophones and amorphous clays in the river. Such trends are coincident with those of low-RSM winter waters and high RSM spring flood waters as observed in Central Siberian rivers (open squares and circles, respectively, in Fig. 5B). The rivers exhibiting the highest RSM are those draining the western Siberia lowlands, which have clay deposits and minimal amounts of crystalline rocks in their watershed (Frey et al., 2007a,b; Pokrovsky et al., 2015a).

The residence time of RSM in rivers is comparable to that of the water itself, i.e., days in small rivers and weeks in largest rivers. The dissolution of silicates with high surface area is rather fast, and that of the plant litter is on the order of hours to days (Fraysse et al., 2010; Jeandel and Oelkers, 2015). As such, this dissolution may not induce significant Si isotope fractionation. The spring river waters are, however, supersaturated with respect to halloysite, imogolite, illite, montmorillonite and kaolinite. Thus secondary Al silicate formation cannot be ruled out. Nevertheless, no statistically significant correlation ($p > 0.05$) was found between river water saturation state with respect to these clay minerals and measured Si isotope ratios. Moreover, there is no evidence for authigenic mineral formation in the RSM in the Nizhnyaya Tunguska River (Pokrovsky et al., 2005), thus the formation of secondary minerals in the river waters seems unlikely.

An additional reason for the low δ^{30}Si composition of rivers draining the western Siberian lowlands is that these regions have a significant proportion of wetlands (i.e. >10%). These wetlands are still frozen during the sampling period and thus do not uptake any Si in vegetation. Instead, they may release isotopically-light Si from vegetation, as there is a weak but statistically significant correlation between δ^{30}Si and wetland proportion ($R^2 = 0.23$ at $p = 0.01$, ESM Fig. S17). The isotopic signature of western Siberia plants is unknown at present. The few available data suggest that δ^{30}Si varies significantly among boreal plants; the Siberian larch has a δ^{30}Si ranging from +1.2 to +1.5‰ (Pokrovsky et al., 2013), whereas Norway spruces and European larches have a δ^{30}Si of +0.2‰ (Engstrom et al., 2008). However, birch, willow, dwarf shrubs, moss and lichens from Sweden, plants common in western Siberia, exhibit even lighter Si isotopic compositions with δ^{30}Si ranging from -0.15 to -0.30 ‰, whereas the humus horizon has a δ^{30}Si = -0.27 ‰ (Engstrom et al., 2008). Therefore, it is possible that, in addition to RSM dissolution, plant litter vegetation leaching of isotopically-light Si during the spring flood may be a factor contributing to the light Si observed in the Kas, Turukhan, and Sym rivers as shown in ESM Fig. 17. Distinguishing

between these two sources of the light Si isotopes to the western Siberian tributaries of the Yenisey River, however, is not possible at present.

5.3. Evaluation of isotopic fluxes to the Arctic Ocean

The Yenisey River is largely representative of the rivers draining to the Arctic Ocean, due to its highly variable lithology, contrasting permafrost, forest, wetland, and vegetation coverage. As such, the results of this study may provide reasonable estimates of the range of dissolved Mg and Si isotope fluxes to the Arctic Ocean. The sample collected from the terminal point of the Yenisey River during spring flood has a $\delta^{30}Si = 1.30\pm0.07‰$. This value compares with the average annual discharge-weighted $\delta^{30}Si$ values of 1.67 and 1.08 ‰ found for the Kochechum and the Nizhnyaya Tunguska rivers of the Central Siberian Plateau (Pokrovsky et al., 2013). The Yenisey spring flood Si isotopic signature is also close to that measured in the boreal permafrost-free Kalix River (+0.7 to +1.5 ‰, Engström et al., 2010) and in large tropical rivers (+0.91±0.09 ‰ in Congo, Hughes et al., 2011; 1.51±0.19 ‰ in Ganges-Brahmaputra system, Georg et al., 2009). In contrast, the $\delta^{30}Si$ of the Siberian rivers are higher than that observed in rivers draining small Iceland catchments (0.63±0.38‰, Georg et al., 2007), and in Swiss rivers (0.84±0.19‰, Georg et al., 2006). Such differences may stem from the significantly lower concentrations of suspended material in Siberian rivers compared to the mountainous Iceland and Switzerland rivers, where enhanced runoff disfavors clay formation, which together with scarcer vegetation, results in lower river water $\delta^{30}Si$.

The $\delta^{26}Mg$ is equal to -1.29±0.03‰ at the mouth of the Yenisey River. This value is very close to that of the Lena River during its summer low flow with a $\delta^{26}Mg=-1.28\pm0.08‰$ (Tipper et al., 2006). This observation suggests that the Mg isotope compositions of Siberian rivers are significantly lighter (i.e. -1.3‰) compared both to seawater (-0.82‰) and to the -

1.09‰ of mean global river runoff (Tipper et al., 2006). We hypothesize that the Mg composition of the Yenisey, as well as the Lena, reflects a significant contribution of isotopically-light, highly reactive Precambrian dolomites, which are abundant in the southern Siberian Platform. In contrast, it is unlikely that the Ob River, draining mainly Quaternary clays and sands covered by peat, will have such a light Mg isotope signature.

If it can be assumed to a first approximation that the flux weight average annual isotopic compositions of Si and Mg can be estimated as the discharge weighted sum of the spring, summer, and winter fluxes one can write:

$$\delta^{30}Si_{annual} = \delta^{30}Si_{\,spring} \times 0.386 + \delta^{30}Si_{\,summer} \times 0.254 + \delta^{30}Si_{\,winter} \times 0.36$$

$$\delta^{26}Mg_{annual} = \delta^{26}Mg_{spring} \times 0.29 + \delta^{26}Mg_{summer} \times 0.265 + \delta^{26}Mg_{winter} \times 0.445$$

where the subscripts "spring", "summer" and "winter" denote the isotopic composition of Yenisey River water during the respected time of the year, whereas the fractions of the annual fluxes for Mg and Si have been calculated after Holmes et al. (2012) and can be found in ESM Table S3. The spring, summer and winter isotopic compositions in this equation are estimated as follows. The isotopic compositions during the spring are taken from the results described above and are equal to 1.30‰ and -1.29‰ for $\delta^{30}Si$ and $\delta^{26}Mg$ respectively. During the summer period, the composition of the Yenisey river is assumed be similar to that of other Central Siberian rivers reported by Pokrovsky et al. (2013) and Mavromatis et al (2014a) and equal to -1.5±0.2‰ and +1.5±0.2‰ for $\delta^{30}Si$ and $\delta^{26}Mg$, respectively. The isotopic compositions of the river water during the winter is estimated from the annual variations of Ninzhaya Tunguska River, the most similar, in terms of lithology, to that of the overall Yenisey basin and dominated by Precambrian dolomite dissolution with pronounced secondary minerals formation in the deep groundwaters (Pokrovsky et al., 2013; Mavromatis et al., 2014a). The resulting mass averaged annual isotope signatures of Si and Mg flux from the Yenisey River to the Arctic Ocean are thereby estimated to be $\delta^{30}Si_{annual} = 1.60\pm0.25‰$ and $\delta^{26}Mg_{annual} = -1.58\pm0.30‰$.

6. Conclusions

Much of the water and solute flux to the Arctic Ocean from the continents occurs during the late spring snow melt. As such the composition of these melt waters have a strong influence on the supply and isotopic composition of dissolved elements to the Arctic Ocean. In this study we presented the chemical compositions and isotopic signatures of Sr, Mg, and Si along Yenisey River and 28 of its large and small tributaries during the late spring flood. Despite the large variation in lithology, vegetation and permafrost coverage in the Yenisey River watershed, the isotopic composition of both dissolved Mg and Si was found to be only weakly influenced by these parameters. These observations suggest that soil mineral formation and element uptake by vegetation is negligible during this time of the year, likely owing to the frozen soil profile. The observed variations of Mg and Si isotope compositions along the Yenisey River can be explained by the mixing of two end-member sources with possible fractionation due to mineral dissolution process. Isotopically light Si and isotopically heavy Mg are likely provided by the dissolution of suspended matter including clay minerals and plant litter leaching. The mobilization of the biogenic and clay pools enrich the river water in Si over Mg (Fig. 6C). Isotopically heavy Si and isotopically light Mg appear to be added from deep underground waters feed to the river via taliks. This second end-member is accompanied by elevated DIC concentrations as well as high Ca/Al, Ca/Si and Mg/Si ratios, consistent with the Mg-bearing carbonate dissolution and secondary silicate precipitation in the deep underground reservoirs.

The average annual isotope signal of river water input to the Arctic Ocean from the Yenisey River is estimated to be -1.58±0.30 and +1.60±0.25 for δ^{26}Mg and δ^{30}Si, respectively. As the Yenisey River is both the largest arriving to the Arctic, and has a representative watershed, these isotopic ratios may approximate the overall dissolved riverine flux to this ocean.

Acknowledgments

References

Albarède F., Michard A, Minster J.F., Michard G. (1981) ^{87}Sr/^{86}Sr ratios in hydrothermal waters and deposits from the East Pacific Rise at 21°N. Earth Planet. Sci. Lett. 55, 229-236.

Alekin O.A. (1970) Foundations of hydrochemistry (Osnovy Gidrokhimii). Gidrometeorological Izd-vo, Leningrad, 444 pp.

Andersen M., Stirling C., Porcelli D., Halliday A., Andersson P., Baskaran M. (2007) The tracing of riverine U in Arctic seawater with very precise ^{234}U/^{238}U measurements. Earth Planet. Sci. Let. 259, 171–185.

Anisimova N. P. (1981) Cryohydrochemical Features of the Permafrost Zone. (Kriogidrokhimicheskie osobennosti merzloi zony). Nauka (in Russian), 152 pp.

Bagard M.L., Chabaux F., Pokrovsky O.S., Prokushkin A.S., Viers, J, Dupré B, Stille P. (2011) Seasonal variability of element fluxes in two Central Siberian rivers draining high latitude permafrost dominated areas. Geochim. Cosmochim. Acta 75, 3335–3357.

Bagard M. L., Schmitt A. D., Chabaux F., Pokrovsky O. S., Viers J., Stille P., Labolle F. and Prokushkin A. S. (2013) Biogeochemistry of stable Ca and radiogenic Sr isotopes in a

larch covered permafrost-dominated watershed of Central Siberia. Geochim. Cosmochim. Acta 114, 169–187.

Beinlich, A., Mavromatis, V., Austrheim, H., Oelkers, E.H. (2014) Inter-mineral Mg isotope fractionation during hydrothermal ultramafic rock alteration – Implications for the global Mg-cycle. Earth Planet. Sci. Lett. 392, 166-176.

Bochkarev, P.F. (1959) Hydrochemistry of rivers of eastern Siberia (Gidrokhimiya rek Vostochnoi Sibiri). Sibirskoe Izd-vo, Irkutsk, 156 pp. (in Russian)

Bourdon, B., Tipper, E.T., Fitoussi, C., Stracke, A. (2010) Chondritic Mg isotope composition of the Earth. Geochim. Cosmochim. Acta 74, 5069-5083.

Brenot, A., Cloquet, C., Vigier, N., Carignan, J., France-Lanord, C., 2008. Magnesium isotope systematics of the lithologically varied Moselle river basin, France. Geochim. Cosmochim. Acta 72, 5070-5089.

Brown, J., Ferrians Jr., O.J., Heginbottom, J.A., Melnikov, E.S. (1998) Revised February 2001 Circum-arctic map of permafrost and ground ice conditions. Boulder, CO: National Snow and Ice Data Center/World Data Center for Glaciology. Digital media. http:// nsidc.org/fgdc/maps/perm_ext_browse.html.

Buffam I., Laudon H., Seibert J., Moerth C-M. Bishop K (2008) Spatial heterogeneity of the spring flood acid pulse in a boreal stream network. Sci. Tot. Environ 407, 708-722.

De la Rocha, C.L., Brzezinski, M.A., Deniro, M.J. (2000) A first look at the distribution of the stable isotopes of silicon in natural waters. Geochim. Cosmochim. Acta 64, 2467–2477.

Engström E., Rodushkin I., Ohlander B., Ingri J., Baxter D.C. (2008) Silicon isotopic composition of boreal forest vegetation in Northern Sweden. Chem Geol. 257, 247-256.

Engström E., Rodushkin I., Ingri J., Baxter D.C., Ecke F., Osterlund H., Ohlander B. (2010) Temporal isotopic variations of dissolved silicon in a pristine boreal river. Chem. Geo. 271, 142-152.

Fraysse, F., Pokrovsky, O.S., Meunier, J.D., 2010. Experimental study of terrestrial plant litter interaction with aqueous solutions. Geochim. Cosmochim. Acta 74, 70-84.

Frey K.E., McClelland J.W., Holmes R.M., Smith L.C. (2007) Impacts of climate warming and permafrost thaw on the riverine transport of nitrogen and phosphorus to the Kara Sea. J. Geophys. Res. 112, G04S58, doi: 10.1029/2006JG000369.

Frey K.E., Siegel D.I., Smith L.C. (2007) Geochemistry of west Siberian streams and their potential response to permafrost degradation. Water Resources Research 43, W03406, doi: 10.1029/2006WR004902.

Georg R.B., Reynolds B.C., West A.J., Burton K.W., Halliday A.N. (2007) Silicon isotope variations accompanying basalt weathering in Iceland. Earth Planet. Sci. Let. 261, 476-490.

Georg R.B., Reynold B.C., Frank M., Halliday A.N. (2006) Mechanisms controlling the silicon isotopic compositions of river waters. Earth Planet. Sci. Let. 249, 290-306.

Georg R.B., West A.J., Basu A.R., Halliday A.N. (2009) Silicon fluxes and isotope composition of direct groundwater discharge into the Bay of Bengal and the effect on the global ocean silicon isotope budget. Earth Planet. Sci. Let, 283, 67-74.

Gordeev V.V., Martin J.M., Sidorov I.S., Sidorova M.V. (1996) A reassessment of the Eurasian river input of water, sediment, major elements, and nutrients to the Arctic ocean. Amer. J. Sci. 296, 664-691.

Gordeev V.V., Rachold V., Vlasova I.E. (2004) Geochemical behavior of major and trace elements in suspended particulate material of the Irtysh river, the main tributary of the Ob river, Siberia. Appl. Geochem. 19, 593-610.

Guo, L., Zhang, J.-Z., Gueguen, C. (2004) Speciation and fluxes of nutrients (N, P, Si) from the upper Yukon River. Global Biogeochemical Cycles 18, GB1038.

Guo, L., Cai, Y., Belzile, C., Macdonald, R. (2012) Sources and export fluxes of inorganic and organic carbon and nutrient species from the seasonally ice-covered Yukon River. Biogeochemistry 107, 187–206.

Gustafsson, J. (1999) WinHumicV for Win95/98/NT: A Windows version of MINTEQA2 http:// www.lwr.kth.se/English /OurSoftware/vminteq/index.htm.

Handler, M.R., Baker, J.A., Schiller, M., Bennett, V.C., Yaxley, G.M. (2009) Magnesium stable isotope composition of Earth's upper mantle. Earth Planet. Sci. Let. 282, 306-313.

Holmes, R.M., McClelland, J.W., Peterson, B.J., Tank, S.E., Bulygina, E., Eglinton, T.I., Gordeev, V.V., Gurtovaya, T.Y., Raymond, P.A., Repeta, D.J., Staples, R., Striegl, R.G., Zhulidov, A.V., Zimov, S.A. (2012) Seasonal and Annual Fluxes of Nutrients and Organic Matter from Large Rivers to the Arctic Ocean and Surrounding Seas. Estuaries Coasts 35, 369-382.

Holmes, R.M., Coe, M.T., Fiske, G.J., Gurtovaya, T., McClelland, J.W., Shiklomanov, A.I., Spencer, R.G.M., Tank, S.E., Zhulidov, A.V. (2013) Climate change impacts on the hydrology and biogeochemistry of Arctic Rivers, In: Climatic Changes and Global warming of Inland Waters: Impacts and Mitigation for Ecosystems and Societies, Eds. C.R. Goldman, M. Kumagi, and R.D. Robarts, John Wiley and Sons, p. 1-26.

Hughes H.J., Sondag F., Cocquyt C., Laraque A., Pandi A., André L., Cardinal D. (2011) Effect of seasonal biogenic silica variations on dissolved silicon fluxes and isotopic signatures in the Congo River. Limnology and Oceanography 56, 551-561.

Huh, Y., Chan, L.-H., Zhang, L., Edmond, J.M., (1998a). Lithium and its isotopes in major world rivers: Implications for weathering and the oceanic budget. Geochim. Cosmochim. Acta 62, 2039-2051.

Huh Y., Panteleyev G., Babich D., Zaitsev A., Edmond J.M. (1998b) The fluvial geochemistry of the rivers of Eastern Siberia: II. Tributaries of the Lena, Omoloy, Yana, Indigirka, Kolyma, and Anadyr draining collisional/accretionary zone of the Verkhoyansk and Cherskiy ranges. Geochim. Cosmochim. Acta 62, 2053-2075.

Huh Y., Edmond J.M. (1999) The fluvial geochemistry of the rivers of Eastern Siberia: III. Tributaries of the Lena and Anabar draining the basement terrain of the Siberian Craton and the Trans-Baikal Highlands. Geochim. Cosmochim. Acta 63, 967-987.

Ilina, S.M., Viers, J., Lapitsky, S.A., Mialle, S., Mavromatis, V., Chmeleff, J., Brunet, P., Alekhin, Y.V., Isnard, H., Pokrovsky, O.S., 2013. Stable (Cu, Mg) and radiogenic (Sr, Nd) isotope fractionation in colloids of boreal organic-rich waters. Chem. Geol. 342, 63-75.

Jeandel, C., Oelkers, E.H., 2015. The influence of terrigenous particulate material dissolution on ocean chemistry and global element cycles. Chem. Geol. 395, 50-66.

Keller K., Blum J.D., Kling G.W. (2010) Stream geochemistry as an indicator of increasing permafrost thaw depth in an arctic watershed. Chem. Geol. 273, 76-81.

Lemarchand D., Gaillardet J. (2006) Transient features of the erosion of shales in the Mackenzie basin (Canada), evidences from boron isotopes. Earth Planet. Sci. Let. 245, 174–189.

Mavromatis, V., Gautier, Q., Bosc, O., Schott, J. (2013) Kinetics of Mg partition and Mg stable isotope fractionation during its incorporation in calcite. Geochim. Cosmochim. Acta 114, 188-203.

Mavromatis, V., Prokushkin, A.S., Pokrovsky, O.S., Viers, J., Korets, M.A. (2014a) Magnesium isotopes in permafrost-dominated Central Siberian larch forest watersheds. Geochim. Cosmochim. Acta 147, 76-89.

Mavromatis, V., Meister, P., Oelkers, E.H. (2014b) Using stable Mg isotopes to distinguish dolomite formation mechanisms: A case study from the Peru Margin. Chem. Geol. 385, 84-91.

Mavromatis, V., Bundeleva, I.A., Shirokova, L.S., Millo, C., Pokrovsky, O.S., Bénézeth, P., Ader, M., Oelkers, E.H. (2015) The continuous re-equilibration of carbon isotope

compositions of hydrous Mg carbonates in the presence of cyanobacteria. Chem. Geol. 404, 41-51.

Millot R., Gaillardet J., Dupre´ B., Allegre C. (2003) Northern latitude chemical weathering rates: clues from the Mackenzie River Basin, Canada. Geochim. Cosmochim. Acta 67, 1305– 1329.

Mitchell T.D., Jones P.D. (2005) An improved method of constructing a database of monthly climate observations and associated high-resolution grids. Int. J. Climatology 25, 693-712.

Oelkers, E.H., Benning, L.G., Lutz, S., Mavromatis, V., Pearce, C.R., Plümper, O., 2015. The efficient long-term inhibition of forsterite dissolution by common soil bacteria and fungi at Earth surface conditions. Geochim. Cosmochim. Acta 168, 222-235.

Opfergelt, S., Burton, K.W., Georg, R.B., West, A.J., Guicharnaud, R.A., Sigfusson, B., Siebert, C., Gislason, S.R., Halliday, A.N. (2014). Magnesium retention on the soil exchange complex controlling Mg isotope variations in soils, soil solutions and vegetation in volcanic soils, Iceland. Geochim. Cosmochim. Acta 125, 110-130.

Opfergelt, S., Georg, R.B., Delvaux, B., Cabidoche, Y.M., Burton, K.W., Halliday, A.N., (2012) Mechanisms of magnesium isotope fractionation in volcanic soil weathering sequences, Guadeloupe. Earth Planet. Sci. Lett. 341–344, 176-185.

Opfergelt, S., Delvaux, B., Andre, L., Cardinal, D. (2008) Plant silicon isotopic signature might reflect soil weathering degree. Biogeochemistry 91, 163-175.

Parkhurst, D.L. and Appelo, C.A.J. (1999) User's guide to PHREEQC (version 2) — a computer program for speciation, batch-reaction, one-dimensional transport, and inverse geochemical calculations. U.S. Geological Survey Water-Resources Investigations Report 99-4259 (310 pp.).

Pearce, C.R., Saldi, G.D., Schott, J., Oelkers, E.H. (2012) Isotopic fractionation during congruent dissolution, precipitation and at equilibrium: Evidence from Mg isotopes. Geochim. Cosmochim. Acta 92, 170-183.

Pearce, C.R., Parkinson, I.J., Gaillardet, J., Charlier, B.L.A., Mokadem, F., Burton, K.W. (2015) Reassessing the stable ($\delta^{88/86}$Sr) and radiogenic (^{87}Sr/^{86}Sr) strontium isotopic composition of marine inputs. Geochim. Cosmochim. Acta 157, 125-146.

Pogge von Strandmann, P.A.E., 2008. Precise magnesium isotope measurements in core top planktic and benthic foraminifera. Geochem. Geophys. Geosyst. 9, 13.

Pogge von Strandmann, P.A.E., Burton, K.W., James, R.H., van Calsteren, P., Gislason, S.R., Sigfusson, B., 2008. The influence of weathering processes on riverine magnesium isotopes in a basaltic terrain. Earth Planet. Sci. Lett. 276, 187-197.

Pokrovsky, B.G., Mavromatis, V., Pokrovsky, O.S. (2011) Co-variation of Mg and C isotopes in late Precambrian carbonates of the Siberian Platform: A new tool for tracing the change in weathering regime? Chem. Geol. 290, 67-74.

Pokrovsky O.S., Schott J. (2002) Iron colloids/organic matter associated transport of major and trace elements in small boreal rivers and their estuaries (NW Russia). Chem. Geol., 190, 141-179.

Pokrovsky O.S., Schott J., Kudryavtzev D.I., Dupré B. (2005) Basalts weathering in Central Siberia under permafrost conditions. Geochim. Cosmochim. Acta 69, 5659-5680.

Pokrovsky O. S., Schott J., Dupré B. (2006) Trace element fractionation and transport in boreal rivers and soil porewaters of permafrost-dominated basic terrain in Central Siberia. Geochim. Cosmochim. Acta 70, 3239-3260.

Pokrovsky O.S., Reynolds B.C., Prokushkin A.S., Schott J., Viers J. (2013) Silicon isotope variations in Central Siberian rivers during basalt weathering in permafrost-dominated larch forests. Chem. Geol. 355, 103–116.

Pokrovsky O.S., Manasypov R.M., Shirokova L.S., Loiko S., Krickov I., Kopysov S., Kolesnichenko L.G., Zemtsov V.A., Kulizhsky S.P., Vorobyev S.N., Kirpotin S.N. (2015a) Permafrost coverage, watershed area and season control of dissolved carbon and major elements in western Siberia rivers. Biogeosciences, 12, 6301–6320.

Pokrovsky, O.S., Manasypov, R.M., Loiko, S., Krickov, I.A., Kopysov, S.G., Kolesnichenko, L. G., Vorobyev, S.N., Kirpotin, S.N. (2015b) Trace elements transport in western Siberia rivers across a permafrost gradient. Biogeosciences Discuss., 12, 17857-17912.

Prokushkin A.S., Pokrovsky O.S., Shirokova L.S., Korets M.A., Viers J., Prokushkin S.G., Amon R., Guggenberger G., McDowell W.H. (2011) Sources and export fluxes of dissolved carbon in rivers draining larch-dominated basins of the Central Siberian Plateau. Envir. Res. Let. 6, 045212.

Tank S.E., Frey K.E., Striegl R.G., Raymond P.A., Holmes R.M., McClelland J.W., Peterson B.J. (2012). Landscape-level controls on dissolved carbon flux from diverse catchments of the circumboreal. Global Biogeochemical Cycles 26, GB0E02, doi: 10.1029/2012GB004299, 2012.

Teng, F.Z., Wadhwa, M., Helz, R.T. (2007) Investigation of magnesium isotope fractionation during basalt differentiation: Implications for a chondritic composition of the terrestrial mantle. Earth Planet. Sci. Lett. 261, 84-92.

Teng, F.Z., Li, W.Y., Ke, S., Marty, B., Dauphas, N., Huang, S.C., Wu, F.Y., Pourmand, A. (2010) Magnesium isotopic composition of the Earth and chondrites. Geochim. Cosmochim. Acta 74, 4150-4166.

Tipper, E.T., Calmels, D., Gaillardet, J., Louvat, P., Capmas, F., Dubacq, B. (2012) Positive correlation between Li and Mg isotope ratios in the river waters of the Mackenzie Basin challenges the interpretation of apparent isotopic fractionation during weathering. Earth Planet. Sci. Lett. 333, 35-45.

Tipper, E.T., Galy, A., Bickle, M.J. (2008) Calcium and magnesium isotope systematics in rivers draining the Himalaya-Tibetan-Plateau region: Lithological or fractionation control? Geochim. Cosmochim. Acta 72, 1057-1075.

Tipper, E.T., Galy, A., Gaillardet, J., Bickle, M.J., Elderfield, H., Carder, E.A. (2006) The magnesium isotope budget of the modem ocean: Constraints from riverine magnesium isotope ratios. Earth Planet. Sci. Lett. 250, 241-253.

Unsworth, E.R., Warnken, K.W., Zhang, H., Davison, W., Black F. , Buffle J., Cao J., Cleven R., Galceran J., Gunkel P., Kalis E., Kistler D., van Leeuwen H.P., Martin M., Noël S., Nur Y., Odzak N., Puy J., van Riemsdijk W., Sigg L., Temminghoff E., Tercier-Waeber M.-L., Toepperwien S., Town R.M., Weng L., Xue H. (2006) Model predictions of metal speciation in freshwaters compared to measurements by in situ techniques, Environ. Sci. Technol. 40, 1942-1949.

Viers J., Prokushkin A.S., Pokrovsky O.S., Kirdyanov A.V., Zouiten C., Chmeleff J., Chabaux F., Oliva P., Dupré B. (2015) Zn isotope fractionation in a pristine larch forest on permafrost-dominated soils in Central Siberia. Geochemical Transactions, 16(1):3.

Vigier N., Bourdon B., Turner S., Allegre C. (2001) Erosion timescales derived from U-decay series measurements in rivers. Earth Planet. Sci. Let. 193, 549–563.

Wadleigh M.A, Veizer J., Brooks C. (1985) Strontium and its isotopes in Canadian rivers: Fluxes and global implications. Geochim. Cosmochim. Acta 49, 1727-1736.

Wimpenny, J., Colla, C.A., Yin, Q.-Z., Rustad, J.R., Casey, W.H. (2014) Investigating the behaviour of Mg isotopes during the formation of clay minerals. Geochim. Cosmochim. Acta 128, 178-194.

Wimpenny, J., Gislason, S.R., James, R.H., Gannoun, A., Pogge Von Strandmann, P.A.E., Burton, K.W. (2010) The behaviour of Li and Mg isotopes during primary phase dissolution and secondary mineral formation in basalt. Geochim. Cosmochim. Acta 74, 5259-5279.

Zakharova, E.A., Pokrovsky, O.S., Dupre, B., Gaillardet, J., Efimova, L.E. (2007) Chemical weathering of silicate rocks in Karelia region and Kola peninsula, NW Russia:

Assessing the effect of rock composition, wetlands and vegetation. Chem. Geol. 242,
255-277.

Figure captions

Figure 1: Sampling stations along Yenisey River and its tributaries. The background color
indicates the extent of permafrost.

Figure 2: Binary molar diagram of Na+K normalized Ca vs. Mg concentrations in river water
samples. The data in the shaded areas were taken from Pokrovsky et al. (2005).
Analytical uncertainties are included in the symbol size.

Figure 3: Plot of $^{87}Sr/^{86}Sr$ ratio versus the percent of basalt in the watershed, as it can be seen
in ESM Table S1.

Figure 4: A) $\delta^{26}Mg$ vs. DIC concentrations in sampled river waters (R^2=0.78; p=0.03). B)
$\delta^{26}Mg$ vs. 1/Mg concentrations in sampled river waters (R^2 = 0.7, p >0.05). The
encircled sample originates from the Yerachimo River that is a tributary of Nizhnyaya
Tunguska River.

Figure 5: A) Plot of $\delta^{26}Mg$ vs. RSM in river water samples (R^2=0.5, p<0.05; $0 \leq RSM \leq 15$
mg/L). The circled sample originates from the Yerachimo River. B) Plot of $\delta^{30}Si$ vs.
RSM in river water samples (R^2=0.81, p<0.05; $0 \leq RSM \leq 15$ mg/L). The open
rectangles and open circles represent values for the Nizhnyaya Tunguska and
Kochechum rivers at the end of the spring flood reported by Pokrovsky et al. (2013)

Figure 6: A) Plot of δ^{30}Si vs. the Ca/Al molar ratio of river water samples. B) Plot of δ^{30}Si vs.

the Ca/Si molar ratio in river water samples. B) Plot of δ^{30}Si vs. the Mg/Si molar ratio

in river water samples.

Table 1 Sampling station and sampling date and basin area of the river discharge

Sampling station	Sampling Date	River name	Latitude	Longitude	Basin area km²	Notes
M20	12.06.2012	Angara	58º04'37.0''	93º0.5'05.1''	754767	
M37	23.06.2012	Angara	51º53'25.0''	104º49'37.3''		starting point from Baikal lake
M14	13.06.2012	Kem'	58º31'00.4''	92º0.5'33.4''	9014	
M23	13.06.2012	Bolshoy Pit	59º02'05.2''	91º44'02.4''	21598	
M27	14.06.2012	Kas	59º57'17.7''	90º33'56.6''	11816	
M5	14.06.2012	Garevka	59º50'58.5''	90º47'45.6''	927	
M12	14.06.2012	Sym	60º15'11.6''	90º02'28.1''	31327	
M11	15.06.2012	Vorogovka	60º48'25.4''	89º51'26.1''	3758	
M4	15.06.2012	Dubches	60º55'36.0''	89º37'11.3''	14661	
M29	17.06.2012	Podkamennaya Tunguska	61º36'51.4''	90º11'08.8''	238699	
M13	18.06.2012	Bakhta	62º28'36.6''	89º01'49.1''	35898	
M26	18.06.2012	Yeloguy	63º11'27.4''	87º44'53.7''	25393	
M32	18.06.2012	Komsa	63º15'15.2''	87º43'40.2''	1667	
M34	19.06.2012	Sukhaya Tunguska	65º10'00.0''	87º59'55.2''	7165	
M9	19.06.2012	Miroedikha	65º36'01.8''	88º03'20.6''	552	
M1	20.06.2012	Turukhan	65º54'23.5''	87º34'52.0''	35726	
M10	21.06.2012	Nizhnyaya Tunguska	65º34'38.9''	90º02'18.4''	441220	
M21	22.06.2012	Kureyka	66º30'07.5''	87º21'25.2''	46600	
M28	24.06.2012	Staraya Igarka	67º24'03.6''	86º27'02.8''	1662	
M31	25.06.2012	Graviyka	67º30'26.3''	86º26'51.0''	323	
M33	25.06.2012	Khantayka	68º06'14.5''	86º39'47.3''	32150	
M17	26.06.2012	Fokina	68º39'23.8''	86º26'14.3''	343	
M6	26.06.2012	Dudinka	69º23'06.3''	86º18'26,8''	5705	
M3	27.06.2012	Malaya Kheta	69º33'51.1''	84º31'31.6''	5942	
M16	27.06.2012	Bolshaya Kheta	69º31'52.5''	84º15'51.6''	20800	
M19	28.06.2012	Sukhaya Dudinka	69º48'14.8''	85º12'01.4''	1903	
M2	21.06.2012	Yerachimo	65º38'21.9''	90º00'51.1''	8870	
M35	21.06.2012	Severnaya	65º57'13.6''	89º01'54.3''	20735	
M7	21.06.2012	Letnyaya	65º55'24.4''	89º02'34.8''	4569	
M30	06.06.2012	Maliy Yenisey	51º26'	95º37'	52878	Upstream Bolshoy Yenisey River - Headwaters
M22	05.06.2012	Maliy Yenisey	51º42'	94º38'	6547	Upstream Bolshoy Yenisey River- Headwaters
M36	12.06.2012	Yenisey 1	58º01'01.3''	93º12'03.0''	304725	Upstream Angara River –After dams
M24	15.06.2012	Yenisey 2	60º54'18.1''	89º41'35.8''	577987	Upstream P. Tunguska
M8	18.06.2012	Yenisey 3	63º15'09.7''	87º41'09.1''	335023	Downstream of P. Tunguska
M18	20.06.2012	Yenisey 4	65º36'04.6''	88º04'43.3''	40770	Upstream N. Tunguska
M25	23.06.2012	Yenisey 5	66º25'07.41''	87º18'03.6''	494304	Downstream of N. Tunguska
M15	27.06.2012	Yenisey 6	69º45'30.6''	84º00'21.5''	156933	Downstream of M. Kheta – at Delta

1 Table 2 Chemical and isotopic compositions of stable Mg and Si and radiogenic Sr in the analyzed samples. The isotopic composition and standard

2 deviation of Mg and Si measurements are based on three replicate analyses. IAPSO seawater analyzed as multi-elemental standard and two full

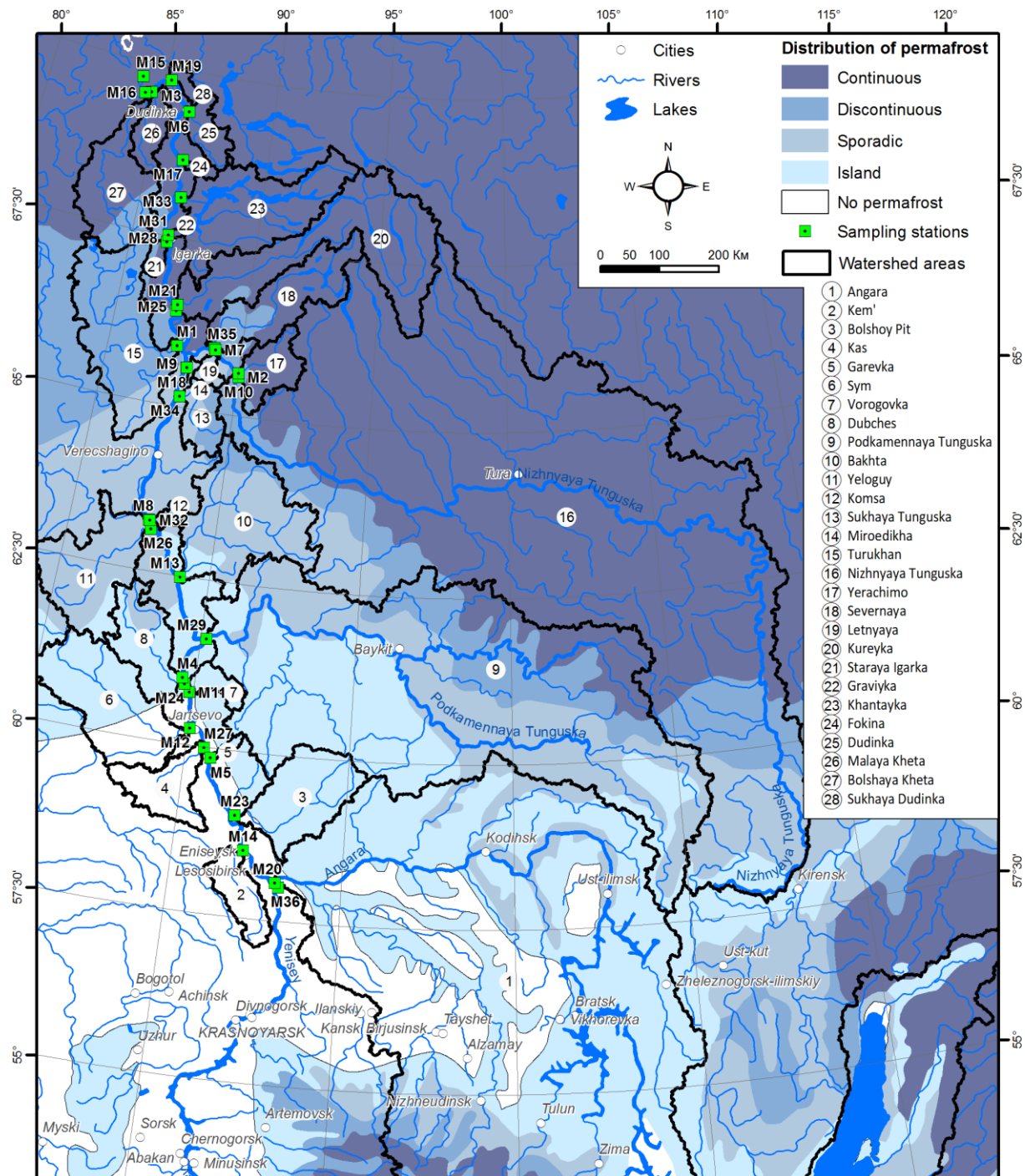3 procedural replicates are reported.

Sampling station	Mg (μM)	δ^{25}Mg (‰)	2σ	δ^{26}Mg(‰)	2σ	Si (μM)	δ^{29}Si (‰)	2σ	δ^{30}Si (‰)	2σ	Sr (μM)	^{87}Sr/^{86}Sr
M20	180.9	-0.75	0.05	-1.48	0.06	41.05	0.71	0.04	1.35	0.12	2.090	0.708854
M37	60.4	-0.75	0.02	-1.46	0.08	24.79	0.68	0.04	1.36	0.01	0.600	0.708859
M14	131.2	-0.66	0.07	-1.33	0.06	45.97	0.84	0.05	1.76	0.03	1.386	0.708368
M23	88.1	-0.75	0.03	-1.46	0.05	73.10	0.63	0.02	1.21	0.03	0.791	0.711712
M27	125.2	-0.61	0.06	-1.19	0.09	149.54	0.41	0.06	0.83	0.14	0.799	0.709552
M5	34.3	-0.51	0.05	-1.03	0.01	102.29	0.66	0.04	1.24	0.04	0.144	0.728101
M12	68.8	-0.50	0.02	-0.99	0.05	133.98	0.40	0.01	0.75	0.01	0.370	0.709473
M11	220.7	-0.89	0.05	-1.73	0.08	48.17	0.86	0.01	1.61	0.04	0.787	0.709974
M4	199.8	-0.53	0.05	-1.04	0.06	152.10	0.61	0.04	1.17	0.08	0.496	0.708902
M29	223.7	-0.78	0.04	-1.54	0.10	87.52	0.56	0.01	1.11	0.08	4.009	0.708926
M13	199.9	-0.67	0.00	-1.29	0.05	82.82	0.81	0.08	1.58	0.08	1.911	0.708501
M26	235.9	-0.61	0.04	-1.23	0.03	127.15	0.63	0.05	1.23	0.11	0.661	0.708502
M32	311.9	-0.71	0.04	-1.41	0.04	49.06	1.12	0.03	2.11	0.09	1.263	0.708649
M34	195.7	-0.70	0.02	-1.35	0.01	89.97	1.01	0.06	1.97	0.04	1.190	0.708547
M9	358.3	-0.84	0.01	-1.64	0.02	71.07	1.03	0.01	2.01	0.06	0.530	0.708626
M1	119.3	-0.55	0.00	-1.09	0.03	61.17	0.48	0.04	0.92	0.06	0.360	0.708875
M10	69.8	-0.46	0.02	-0.88	0.02	105.92	0.71	0.05	1.40	0.08	0.602	0.708312
M21	95.7	-0.58	0.01	-1.13	0.05	70.53					0.725	0.708037
M28	107.3	-0.62	0.01	-1.25	0.04	59.71					0.271	0.708776
M31	119.5	-0.64	0.01	-1.30	0.01	43.87	0.62	0.04	1.22	0.07	0.331	0.708730
M33	123.3					47.46					1.777	0.708502
M17	102.9	-0.71	0.02	-1.37	0.04	47.25	0.72	0.02	1.32	0.05	0.711	0.708394
M6	95.3	-0.58	0.01	-1.11	0.04	57.86					0.251	0.708370
M3	86.5	-0.46	0.02	-0.91	0.10	48.35	**0.70**		**1.29**		0.157	0.708917
M16	56.1	-0.59	0.05	-1.15	0.01	44.97	0.66	0.03	1.27	0.02	0.128	0.708776
M19	55.7	-0.59	0.06	-1.15	0.09	40.48	0.67	0.11	1.29	0.23	0.132	0.708663
M2	162.8	-0.42	0.03	-0.81	0.02	104.46	0.81	0.02	1.60	0.04	1.400	0.708380
M35	61.8	-0.57	0.06	-1.17	0.04	76.23	0.91	0.06	1.72	0.08	0.404	0.707781
M7	387.5	-0.80	0.06	-1.62	0.07	92.43	0.95	0.06	1.88	0.10	3.489	0.708772

M30	132.5	-0.86	0.01	-1.68	0.01	61.60	0.54	0.11	1.10	0.21	1.251	0.708470
M22	142.8	-0.77	0.06	-1.49	0.03	66.69	0.63	0.02	1.14	0.03	1.287	0.708404
M36	119.2	-0.67	0.01	-1.30	0.02	55.76	0.78	0.06	1.49	0.06	1.386	0.708280
M24	127.8	-0.72	0.01	-1.42	0.01	76.16	0.60	0.03	1.13	0.13	1.162	0.708811
M8	167.2	-0.65	0.01	-1.28	0.00	66.76	0.74	0.02	1.43	0.03	1.415	0.708890
M18	141.7	-0.72	0.01	-1.44	0.05	56.54	0.77	0.05	1.47	0.05	1.582	0.708927
M25	10.5	-0.67	0.02	-1.32	0.03	81.61	0.77	0.04	1.53	0.06	1.062	0.708693
M15	98.8	-0.65	0.05	-1.29	0.03	58.39	0.67	0.03	1.30	0.07	0.816	0.708763
IAPSO Seawater (1)		-0.42										
			0.03	-0.85	0.03							
IAPSO Seawater (2)		-0.44	0.04	-0.86	0.04							

4

5

6　　Figure 1

Distribution of permafrost

○ Cities

Rivers

Lakes

Continuous

Discontinuous

Sporadic

Island

No permafrost

■ Sampling stations

▢ Watershed areas

N
W E
S

0 50 100 200 Км

① Angara
② Kem'
③ Bolshoy Pit
④ Kas
⑤ Garevka
⑥ Sym
⑦ Vorogovka
⑧ Dubches
⑨ Podkamennaya Tunguska
⑩ Bakhta
⑪ Yeloguy
⑫ Komsa
⑬ Sukhaya Tunguska
⑭ Miroedikha
⑮ Turukhan
⑯ Nizhnyaya Tunguska
⑰ Yerachimo
⑱ Severnaya
⑲ Letnyaya
⑳ Kureyka
㉑ Staraya Igarka
㉒ Graviyka
㉓ Khantayka
㉔ Fokina
㉕ Dudinka
㉖ Malaya Kheta
㉗ Bolshaya Kheta
㉘ Sukhaya Dudinka

M15 M19 M16 M3 M28 M6 M25 M17 M24 M33 M31 M22 M28 M21 M25 M1 M35 M7 M9 M18 M2 M34 M10 M8 M32 M26 M13 M29 M4 M24 M11 M27 M12 M5 M23 M14 M20 M36

Dudinka
Igarka
Verecshagino
Tura · Nizhnyaya Tunguska
Baykit
Podkamennaya Tunguska
Jartsevo
Kodihsk
Ust-ilimsk
Kirensk
Eniseysk
Lesosibirsk
Yenisey
Angara
Ust-kut
Zheleznogorsk-ilimskiy
Bogotol
Achinsk
Divnogorsk
Ilanskiy
Tayshet
Bratsk
Vikhorevka
Uzhur
KRASNOYARSK
Kansk Birjusinsk
Alzamay
Nizhneudinsk
Tulun
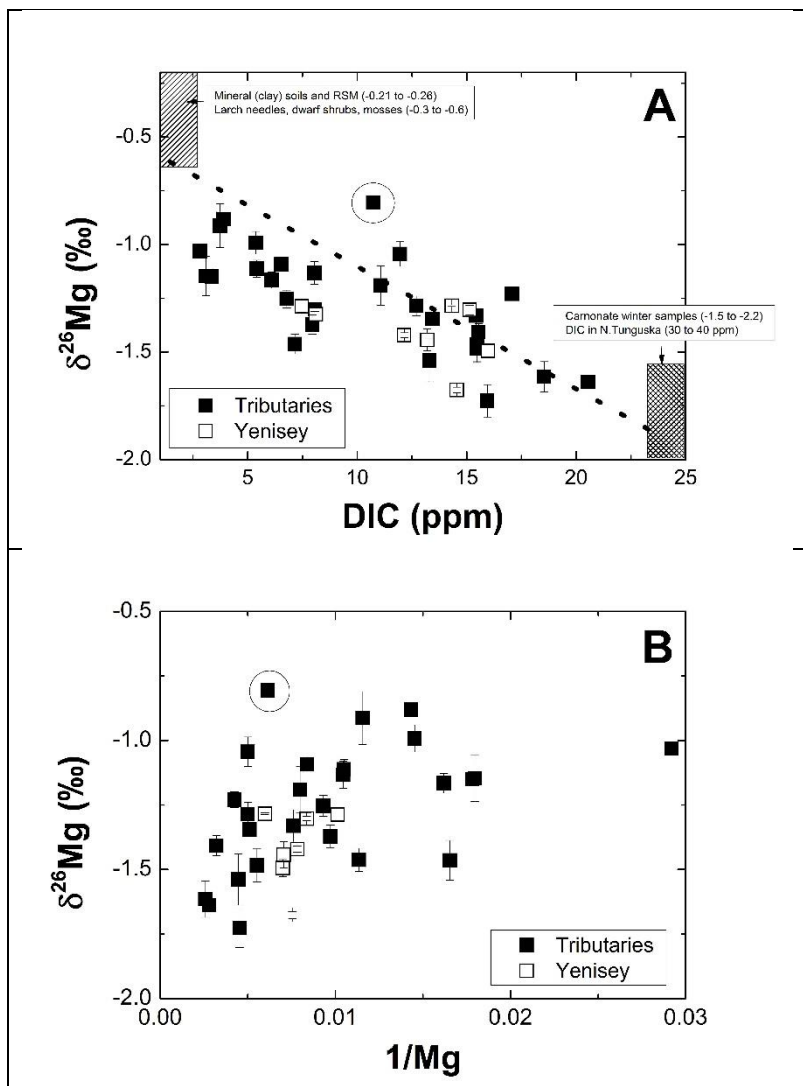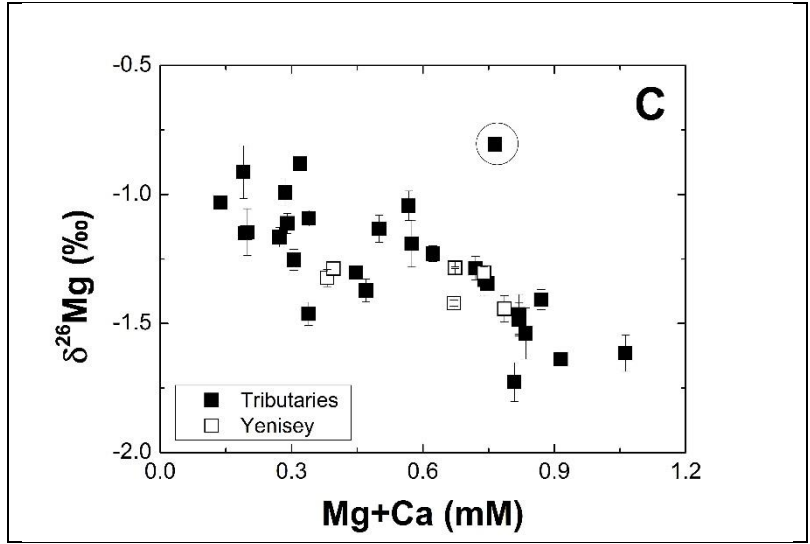Zima
Myski
Sorsk
Chernogorsk
Artemovsk
Abakan Minusinsk
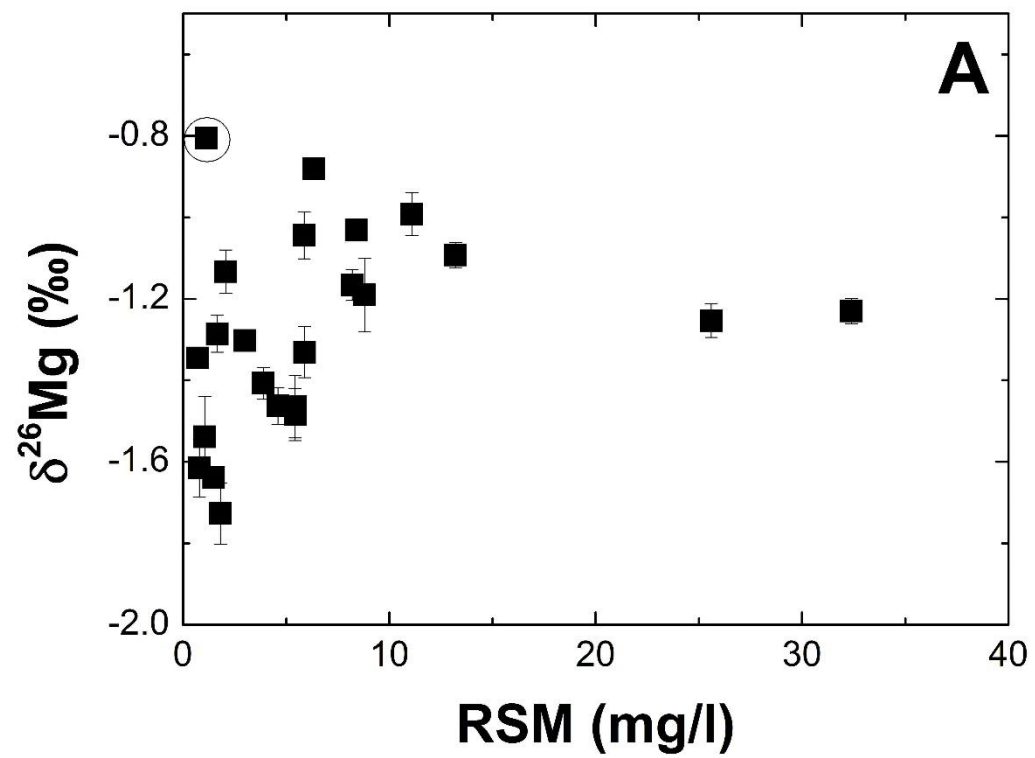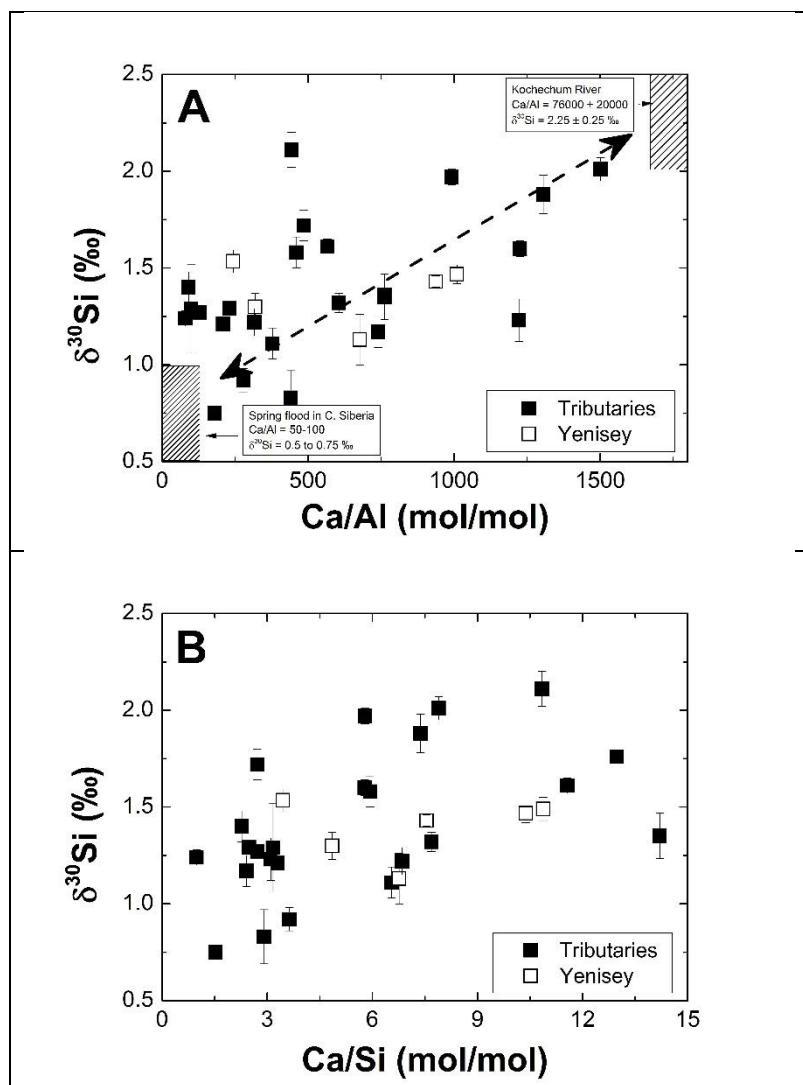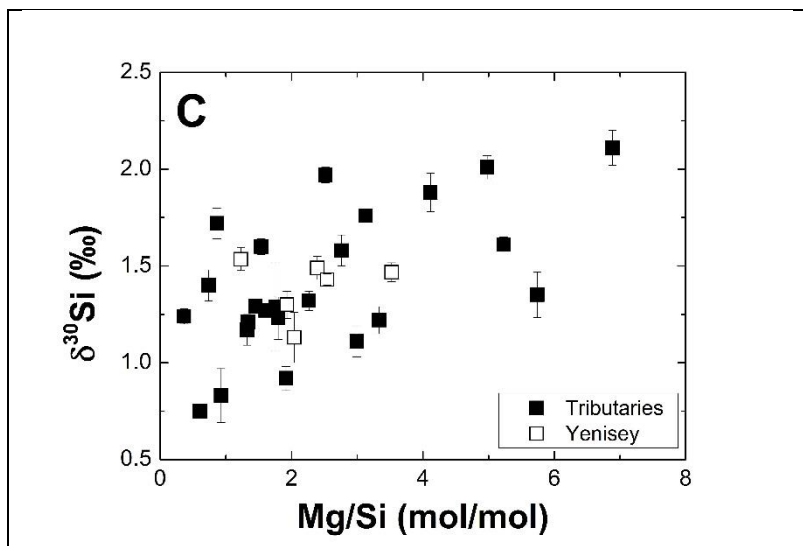Nizhnyaya Tunguska

8

9   Figure 2

10

11

12

13   Figure 3

14

15

16   Figure 4

17

21

22

23

24